A Damping Treatment for Resonant Test Fixtures [1]

F. Cericola, J. D. Rogers, and D. J. Segalman
Sandia National Laboratories
Albuquerque, New Mexico 87185
(505) 846-3633

Abstract

The application of a synthetic putty as a vibration damping treatment has been investigated. The putty was applied to rod specimens of several lengths to obtain frequency characteristics of the treatment. Test results were compared with analyses for the various rod lengths and putty shapes.

Up to 1% damping was achieved with various combinations of viscoelastic plug and elastic rod. The analytic method, though simplistic, did provide guidance to interpreting the results. The analytic method and the experiments, together, established the inertial nature of the dissipative mechanism.

[1]This work was supported by Sandia National Laboratories under contract to the U.S. Department of Energy (DE-AC04-76DP00789).

Contents

1. Introduction

A common problem in vibration testing is the control of a test through a resonant test fixture. If the resonant mode of the test fixture is lightly damped, the control of the test near this frequency is difficult, if not impossible. Thus, methods for moving modal frequencies out of the test bandwidth or sufficiently damping these modes are of great interest to the test engineer. In many cases, it is not possible to remove the fixture resonances from the frequency bandwidth of the test, so one must attempt to damp the fixture sufficiently to allow control through the resonances.

One method for adding damping to a fixture is to apply a viscoelastic material to the surface of the fixture. The mechanical energy transmitted from the fixture to the viscoelastic material is partially dissipated, thus increasing the damping of the fixture.

In the current work, the effect of applying a synthetic putty to the surface of a rod specimen was considered. Aluminum rod specimens of varying lengths were used to obtain frequency dependent characteristics of the damping treatment. The rods had a plug of the putty attached to one end and were impacted at the other end with an instrumented hammer. The damping was identified by the logarithmic decrement from an attached accelerometer and by a modal curve fit. The plugs of putty were applied in two shapes to investigate shape effects and two volumes to investigate volume effects. Viscoelastic properties of the putty were obtained from rheological tests, and a computer code was written to predict the damping for the various plug shapes.

The damping material selected for this investigation was Scotch Seal 1279, a synthetic putty designed for use in sealing environmental test chambers. The damping properties of this material were not available from the manufacturer so tests were performed in the rheology laboratory at Sandia National Laboratories to obtain the master curve shown in Fig. 1. The complex elastic modulus was deduced from the shear storage and loss moduli, recognizing that the material was above its glass-transition at all frequencies. It is clear from the figure that the material's characteristics are a strong function of frequency. Under static loading, the elastic modulus becomes quite small and the material is soft, pliable, and "sticky" to the touch. This is not surprising since it was designed to seal environmental chambers. The frequency range of interest in this work, however, was the range from 2000 Hz to 4000 Hz. In this range, the material has an elastic modulus about one one-thousandth that of aluminum.

2. Discussion of Testing

The tests performed in this work utilized aluminum rod specimens varying from 24 to 48 inches in length, each rod with a 0.75 inch diameter. To these rods were added four different "plugs" of the synthetic putty. The plugs were of two masses, 6 grams and 19.1 grams, and two shapes, cylindrical and conical. The putty plugs were attached to one end of each rod and the rod was then struck at the other end with an instrumented hammer. The input force and the resulting acceleration of the rod were measured using piezoelectric transducers on the hammer and rod respectively. The test configuration is shown in Fig. 2.

The natural frequency and damping ratio were obtained from a modal analysis complex exponential curve fit. The damping ratio was also obtained from the logarithmic decrement technique applied to the measured accelerometer response. The values of the damping ratio obtained in these two manners compared quite well in all cases. The natural frequencies and damping ratios are given in Table 1.

The thrust of this work was to investigate the effect of adding synthetic putty on the damping of the aluminum rods so the natural frequency information appears to be superfluous. However, the natural frequency data provided a method for gaining an understanding of the physical mechanisms present. The initial assumption is that the putty will act as a lossy mass, i.e., a mass and damper combination. However, when Table 1 and Fig. 3 are considered this model is clearly not reasonable. The data show that the rods with 6 grams of putty added had lower natural frequencies than those with 19.1 grams of putty added. This result is not consistent with the lossy mass model, since by that model, increasing the mass should decrease the natural frequency.

If the putty plug is modeled as a spring-mass addition to the rod, the effective end condition on the rod is either mass-like or spring-like depending upon the natural frequencies of the rod and spring-mass system, as shown by Snowdon [5]. For example, if the natural frequency of the rod is much less than that of the spring-mass system then the end condition is mass-like. This concept extends to considering the plug as a viscoelastic addition to the aluminum rod. To gain some understanding of this, the cylindrical plugs were considered as elastic rods attached to the aluminum rods. The elastic properties were obtained from Fig. 1. The natural frequencies obtained from the closed form wave equation for the bi-material rod for the case of the 42 inch aluminum rod and cylindrical putty lengths encompassing all test cases are shown in Fig. 4. The figure also shows the predicted natural frequencies for the simple added mass model. Clearly, the putty plugs acted as rod-like additions in their effect on the natural frequency of the rods.

3. Analysis

The system under test was modeled as an elastic rod attached to a linearly viscoelastic rod of tapering cross-section. The tapering was assumed to be sufficiently gradual that only axial deformations would result.

The resulting computational problem is that of evaluating the dynamic impedance at the driving point of a rod of linearly viscoelastic material, and then finding the complex frequency at which the impedance matches that of the elastic rod to which the viscoelastic rod is attached.

Letting

$$u(x,t) = Im\{e^{i\lambda t}U(x,\lambda)\} \tag{1}$$

and

$$\sigma(x,t) = Im\{e^{i\lambda t}E^*(\lambda)U(x,\lambda)_{,x}\} \tag{2}$$

the equation for extensional vibration of the viscoelastic rod becomes:

$$(A(x)\,E^*(\lambda)\,U(x,\lambda)_{,x})_{,x} + A(x)\,\lambda^2\,\rho\,U(x,\lambda) = 0 \tag{3}$$

subject to the no-stress boundary condition on the right:

$$E^*(\lambda)U(x,\lambda)_{,x}\,|_{x=L} - M\lambda^2 U(x,\lambda)_{x=L} = 0 \tag{4}$$

and the matched-displacement condition on the left:

$$U(x,\lambda)|_{x=0} = 1 \tag{5}$$

In the above, $u(x,t)$ is the axial rod displacement at time t and location x;
$\sigma(x,t)$ is the axial stress at t and x;
$A(x)$ is the cross-sectional area at x;
M is whatever mass is attached to the free end of the rod;
λ is the complex frequency;
$E^*(\lambda)$ and ρ are the complex Young's modulus and density;
and L is the length of the viscoelastic rod.

The notion of complex modulus is discussed in Ref. [2].

The solution, $U(x,\lambda)$, of Equation 3 subject to the boundary conditions of Equations 4 and 5 for a given complex frequency λ defines a dynamic impedance

$$F_v(\lambda) = E^*(\lambda)\,U(x,\lambda)_{,x}\,|_{x=0} / U(x,\lambda)|_{x=0} \tag{6}$$

at the driving point of the rod. It is the matching of this impedance to a corresponding impedance of the attached elastic rod which defines the complex eigenfrequencies of the combined system.

Numerical solution of Equation 3 subject to its boundary conditions at $x = 0$ and $x = L$ at a given complex frequency λ is straight-forward provided that $E^*(\lambda)$ is known.

Using a standard Galerkin formulation to discretize Equation 3 where U is represented as

$$U(x,\lambda) = \sum_{nodes\ n} U_n(\lambda) h_n(x) \tag{7}$$

one obtains for each basis function $h_n(x)$:

$$0 = \int_0^L \{ h_n(x)\ (A(x)\, E^*(\lambda)\, U_{,x})_{,x} + h_n(x)\, \lambda^2\, \rho\, U(\lambda) \}\, dx \tag{8}$$

(Ref. [1] contains a good discussion of these methods.) After substitution of Equation 7 into the above equation, and an integration-by-parts, the following system of equations involving the nodal variables U_m is obtained (one equation for each "n"):

$$\begin{aligned} 0 \;=\; & h_n(L)\, A(L)\, E^*(\lambda)\, U(x,\lambda)_{,x}\,|_{x=L} \\ & - h_n(0)\, A(0)\, E^*(\lambda)\, U(x,\lambda)_{,x}\,|_{x=0} \\ & + \sum_{nodes\ m} \int_0^L \{ -E^*(\lambda)\, h_n(x)_{,x}\ (A(x)\, h_m(x))_{,x}\, U_m(\lambda) \\ & \qquad + A(x)\, \lambda^2\, \rho\, h_n(x)\, h_m(x)\, U_m \}\, dx \end{aligned} \tag{9}$$

The boundary conditions (Equations 4 and 5) are integrated into the above system of equations as follows: occurrences of $E^*(\lambda)\, U(x,\lambda)_{,x}\,|_{x=L}$ are replaced by $M\lambda^2 U(x,\lambda)_{x=L}$; and the equation associated with the node at $x = 0$ is replaced by the boundary condition of Equation 5. Occurrences of $U(x,\lambda)_{x=L}$ and $U(x,\lambda)_{x=0}$ are replaced by the corresponding sums of Equation 7.

In our numerical implementation of the above system of equations, the traditional tent-shaped basis functions are used and a tridiagonal system of equations with complex coefficients results. Solution of that system of equations provides the displacement field $U(x,\lambda)$ as represented in Equation 7, which when substituted into Equation 6, provides numerical values for $F_v(\lambda)$ for the complex frequency, λ, considered.

The impedance of the attached elastic rod is:

$$F_e(\lambda) = -(A_e E_e / L_e)\, (r\,\lambda)\, tan(r\,\lambda) \tag{10}$$

where A_e is the cross-sectional area of the elastic rod;
E_e is the Young's modulus of the elastic rod;
L_e is the length of the elastic rod;
$r = L_r\sqrt{\rho_e/E_e}$;
and ρ_r is the density of the elastic rod.

One would impose a force balance between the elastic rod and the viscoelastic plug by requiring that

$$F_e(\lambda) = F_v(\lambda) \tag{11}$$

and solving for the complex frequency λ that makes Equation 11 true. Such a frequency would be an eigen frequency of the combined system. In the above equation, $F_e(\lambda)$ is evaluated to make proper sense of the sign of the axial force.

At this point, it is necessary to introduce two serious assumptions.

- Since $E^*(\lambda)$ is known for only real λ, the following assumption is invoked:

$$F_v(\lambda) = F_v(Re\{\lambda\}) \tag{12}$$

(Note that though the argument in the above equation is real, the resulting impedance is still complex.)

- Since the mass of the plug is very small compared to that of the rod, we further assume that the system eigen frequency will be close enough to that of the rod alone(ω_{rod}), that we may assume that

$$F_v(\lambda) = F_v(\omega_{rod}) \tag{13}$$

The resulting approximate equation:

$$F_e(\lambda) = F_v(\omega_{rod}) \tag{14}$$

is solved for λ with a Newton iteration.

We hope to remove the above simplifications in future work, using analytic continuation to estimate complex moduli at complex frequencies from the storage and loss moduli of real frequencies.

It is emphasized that the above Fourier technique is not the damping matrix method of Ref. [4] in which a "small viscoelasticity" assumption is invoked.

4. Discussion of Results

The comparisons between the test and analysis results for both natural frequency and damping ratio are shown in Figures 5-10. The natural frequency results, shown in Figures 5 and 6, indicate that the analysis was very good in predicting the natural frequency except for the case of the 6 gram cone. The code predicted that the 6 gram putty cone would have a resonance at about 3000 Hz which the test did not reveal. The authors do not feel that this is due to a serious error in the modeling of the physical mechanism, but probably is an error in the geometric modeling of the cones. The modeling of the large cone was not as critical as the small cone since the large cone did not have a resonance in the frequency band of interest.

The test results for the damping ratio are shown in Figures 7 and 8. These figures compare equal masses of putty applied as cylinders and cones. In each case, the cones provided more damping than did an equal mass of putty shaped as a cylinder. The comparisons between test and analysis results for the damping ratios are shown in Figures 9 and 10. The analysis predicted the trends for all cases except for the 6 gram cone. Just as with the natural frequency comparison, the model predicted a resonance of the 6 gram cone at about 3000 Hz which was not observed in the tests. The analysis did predict the higher damping of the cones which was observed in the tests; however, a physical interpretation of this result has not been obtained. The analytically predicted damping ratios did not agree precisely in magnitude with the test results. The predictions were generally larger than the test values, occasionally by as much as a factor of three. These discrepancies can be attributed to uncertainties in the values of the material properties and to approximations in the modeling. We do not feel that they indicate severe errors in the analysis.

The damping of the aluminum rods without any putty was quite small. The damping ratios obtained for the bare aluminum rods were about 0.0001. This value is consistent with Zener Thermal Relaxation Theory [6] and with test data from Rogers [3]. Comparing this value with the damping ratios shown in Table 1, it is clear that the putty significantly increased the damping of the rods.

5. Conclusions

The current work may be summarized with a few conclusions. First, the addition of the synthetic putty does add damping to the aluminum rods, and the putty plug may be adequately modeled as a viscoelastic addition to the rod. Second, the shape of the putty plug is important for the amount of damping obtained. Conical shapes give greater damping for a given mass of putty than do cylindrical shapes.

This damping mechanism is distinct from methods such as the constrained layer method in that it depends on inertial loads to cause the strains in the viscoelastic material. The viscoelastic material is optimally placed at a location of maximal acceleration on the main structure, not necessarily at a location of high strain. Such a placement was demonstrated in the experiments described here.

That the viscoelastic plug is most effective as a damper when its natural frequency is close to that of the rod, and that the plug's impedance changes drastically with frequency near its own resonance, undermine the utility of the assumptions which are embodied in Equation 13. Future work will be aimed toward removing these assumptions, to solve the full nonlinearity of Equation 11.

6. Acknowledgments

The authors wish to thank Mr. Doug Adolph and Mr. Arlo Nord of Sandia National Laboratories for their efforts in obtaining the master curve for the synthetic putty and in the modal parameter extraction respectively.

References

[1] Cook, R. D., *Concepts and Applications of Finite Element Analysis*, (Second Edition), John Wiley and Sons, New York, 1981, Chapter 18.

[2] Ferry, J. D., *Viscoelastic Properties of Polymers*, (Third Edition), John Wiley and Sons, New York, 1980, p. 68, Equations 39 and 40.

[3] Rogers, J. D., *A Method for Determining Material Damping from Driving Point Measurements,* Ph.D. Dissertation, Iowa State University, Ames, IA, 1986.

[4] Segalman, D. J., "Calculation of damping matrices for linearly viscoelastic structures", *Journal of Applied Mechanics*, Vol. 109, September 1987, pp. 585-588.

[5] Snowdon, J. C., *Shock in Damped Mechanical Systems.* John Wiley and Sons, New York, 1968.

[6] Zener, C., *Elasticity and Anelasticity of Metals,* Univ. of Chicago Press, Chicago, 1948.

7. Tables and Figures

Rod Length (inches)	Mass of Putty (grams)	Shape of Putty	Natural Frequency (Hz)	Damping Ratio	Undamped Natural Freq. (Hz)
24	19.1	Cylinder	4086	0.011	4108
24	19.1	Cone	4076	0.0088	4108
24	6.0	Cylinder	4055	0.0065	4108
24	6.0	Cone	4058	0.0085	4108
30	19.1	Cylinder	3281	0.0102	3294
30	19.1	Cone	3275	0.0088	3294
30	6.0	Cylinder	3258	0.0027	3294
30	6.0	Cone	3259	0.0043	3294
36	19.1	Cylinder	2729	0.0084	2740
36	19.1	Cone	2726	0.0093	2740
36	6.0	Cylinder	2715	0.0022	2740
36	6.0	Cone	2716	0.0028	2740
42	19.1	Cylinder	2340	0.0080	2348
42	19.1	Cone	2336	0.0100	2348
42	6.0	Cylinder	2330	0.0015	2348
42	6.0	Cone	2331	0.0025	2348
48	19.1	Cylinder	2045	0.0085	2052
48	19.1	Cone	2042	0.0100	2052
48	6.0	Cylinder	2038	0.0010	2052
48	6.0	Cone	2038	0.0015	2052

Table 1. Test results for natural frequency and damping ratio.

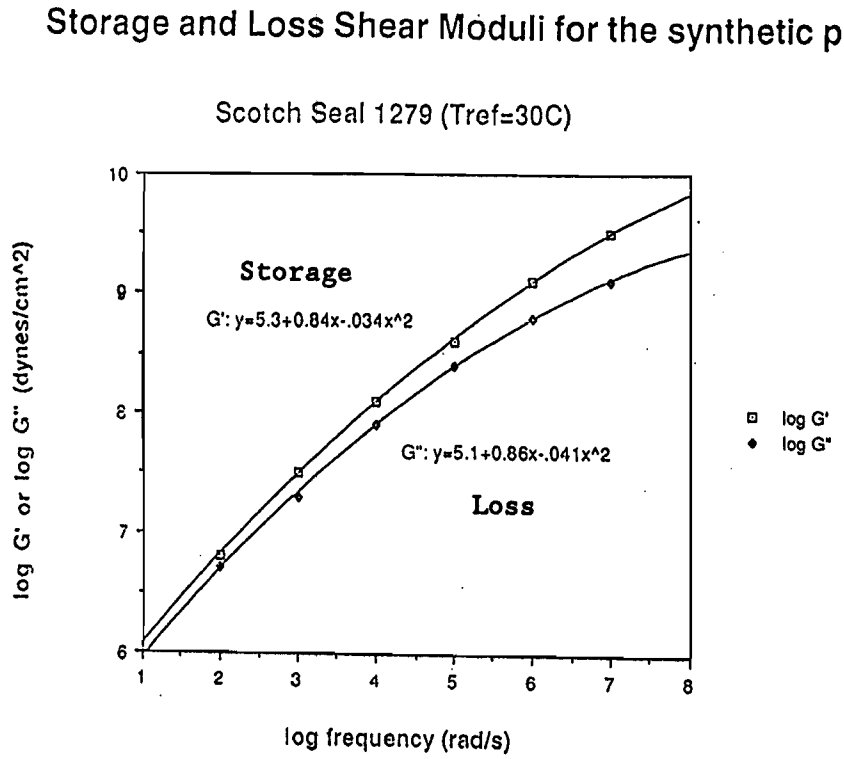

Figure 1. Master curve for the synthetic putty.

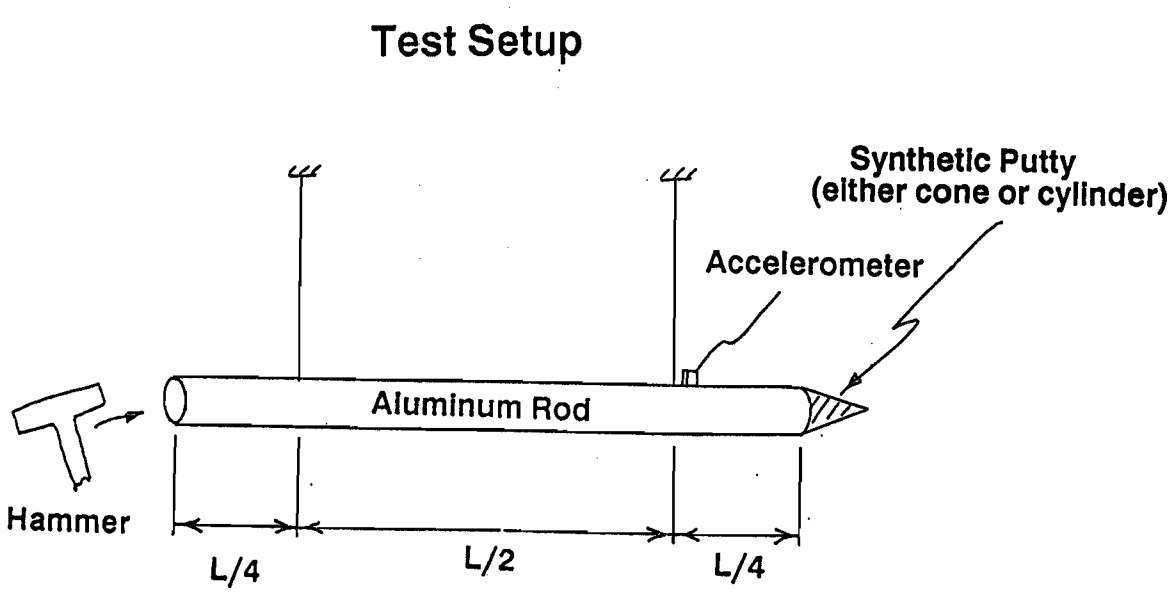

Figure 2. Test configuration.

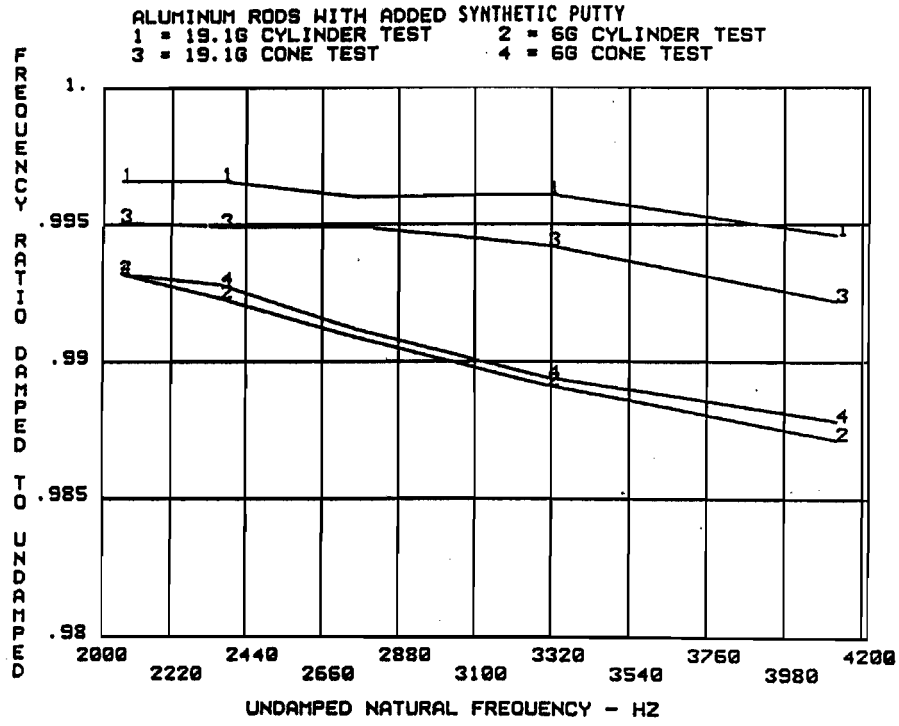

Figure 3. Natural frequency comparison for all tests.

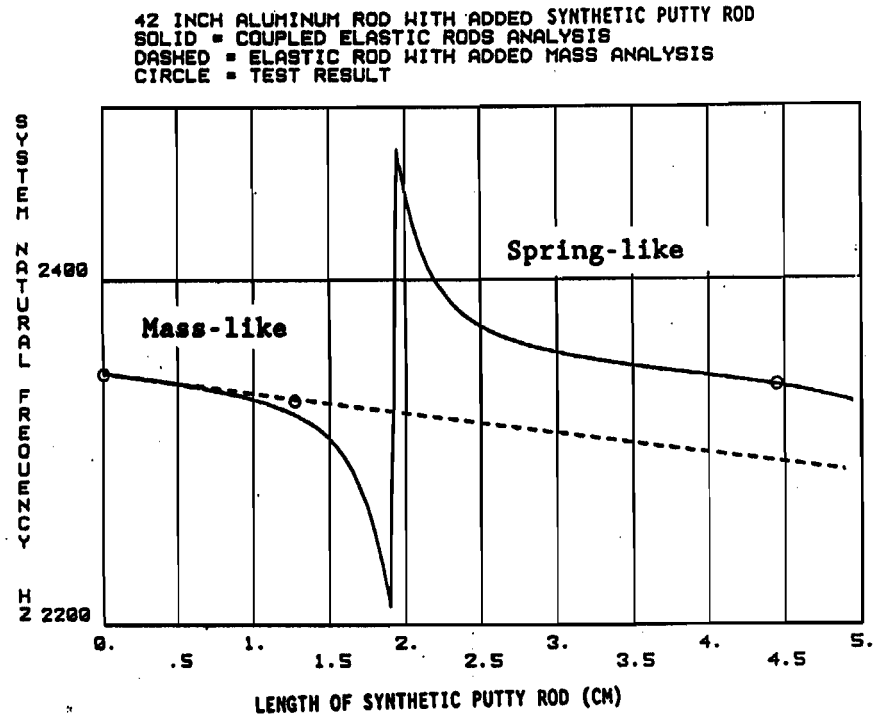

Figure 4. Natural frequencies for test, mass model, and elastic rod model.

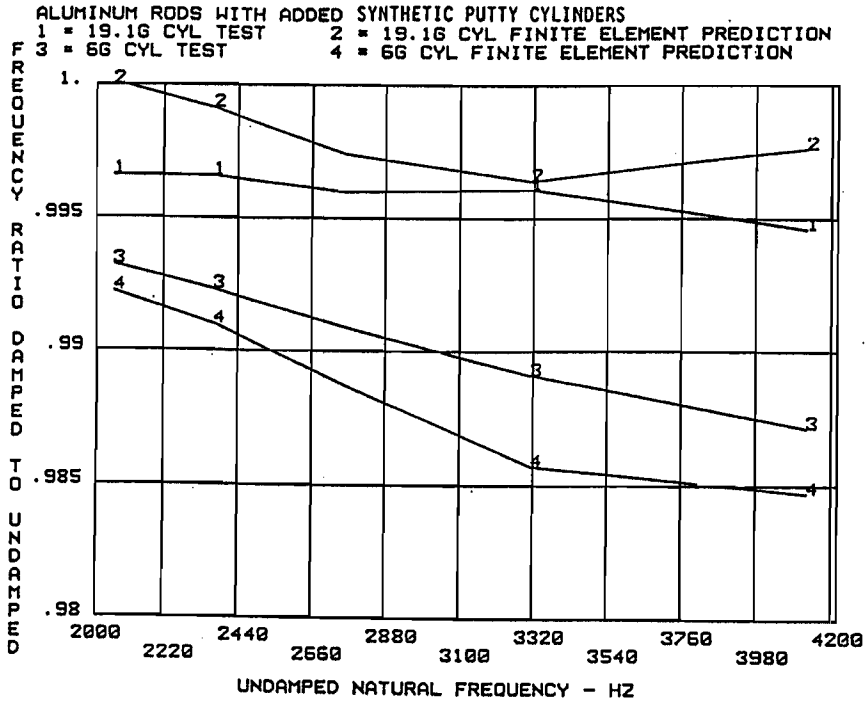

Figure 5. Comparison of frequency prediction of model with test for cylinders.

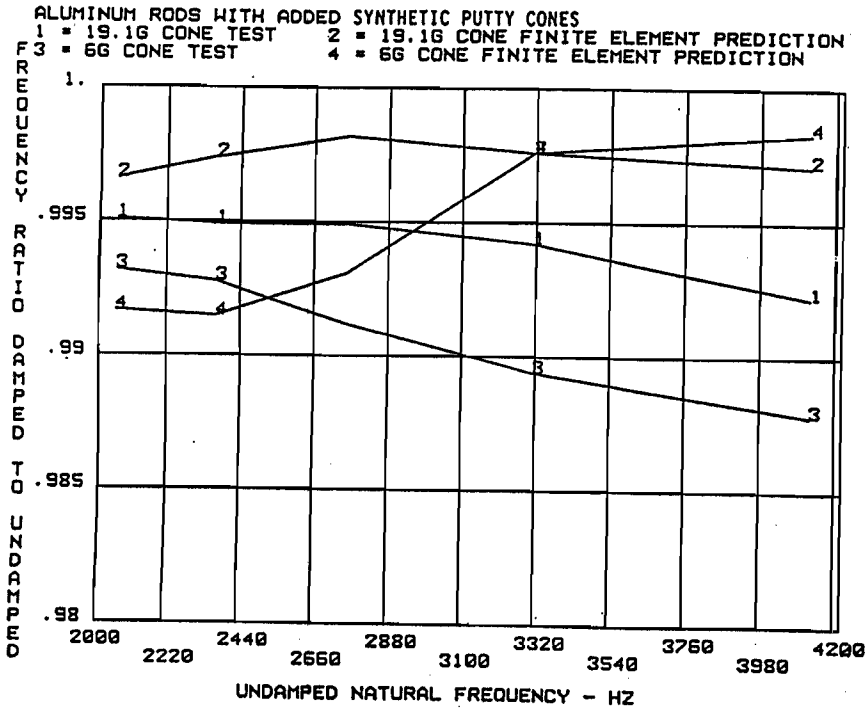

Figure 6. Comparison of frequency prediction of model with test for cones.

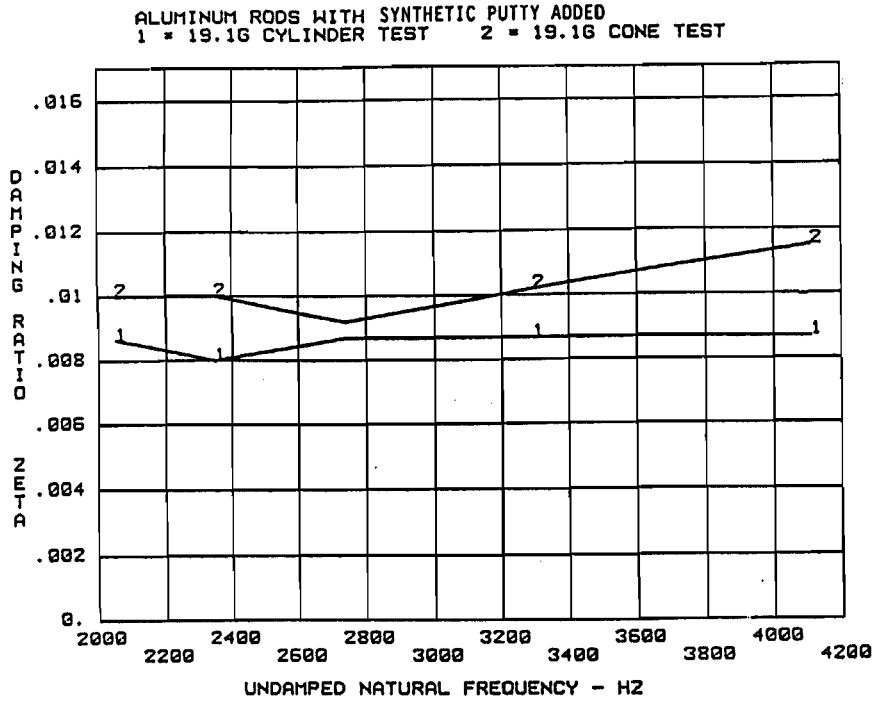

Figure 7. Damping ratios for rods with 19.1 grams of putty.

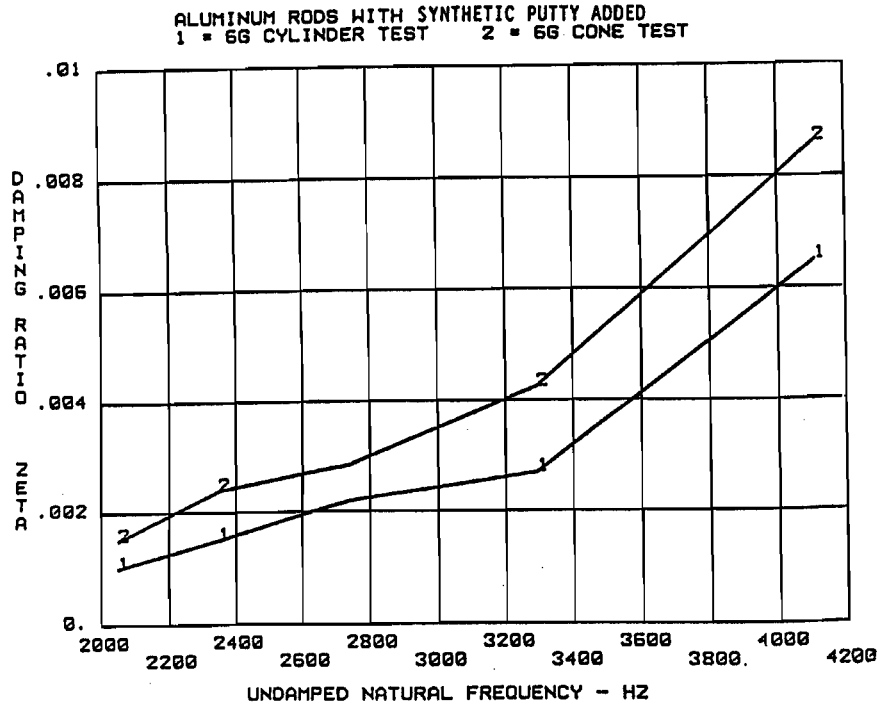

Figure 8. Damping ratios for rods with 6 grams of putty.

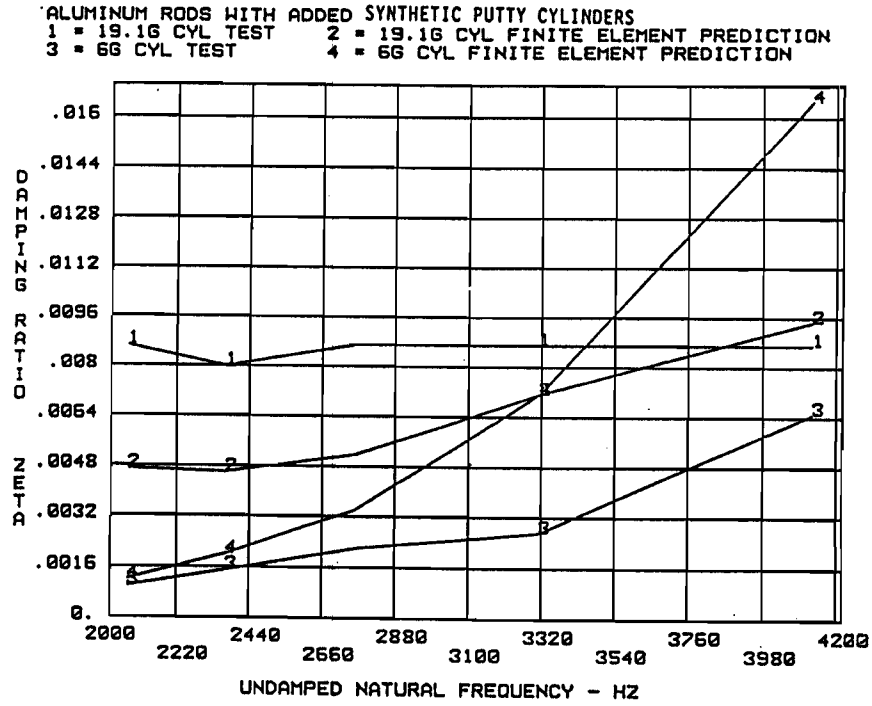

Figure 9. Comparison of damping ratios between test and model for cylinders.

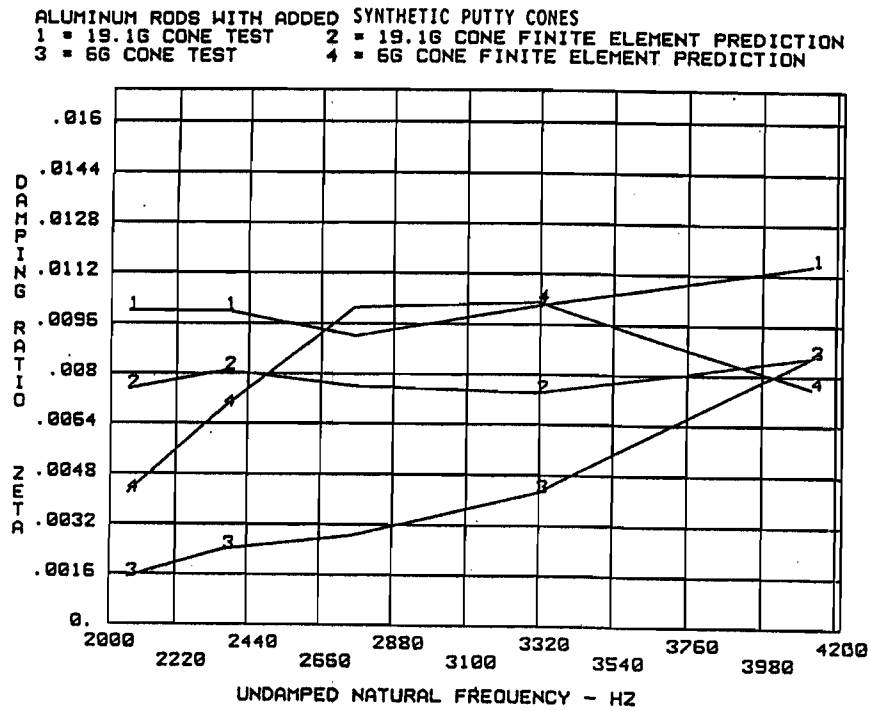

Figure 10. Comparison of damping ratios between test and model for cones.